Characterization of the Interstitial Lung Diseases via Density-Based and Texture-Based Analysis of Computed Tomography Images of Lung Structure and Function[1]

Eric A. Hoffman, PhD, Joseph M. Reinhardt, PhD, Milan Sonka, PhD, Brett A. Simon, MD, PhD, Junfeng Guo, PhD
Osama Saba, MS, Deokiee Chon, MS, Shaher Samrah, MD, Hidenori Shikata, PhD, Juerg Tschirren, PhD
Kalman Palagyi, PhD, Kenneth C. Beck, PhD, Geoffrey McLennan, MD, PhD

Rationale and Objectives. Efforts to establish a quantitative approach to the computed tomography (CT)-based characterization of the lung parenchyma in interstitial lung disease (including emphysema) has been sought. The accuracy of these tools must be site independent. Multi-detector row CT has remained the gold standard for imaging the lung, and it provides the ability to image both lung structure as well as lung function.

Material and Methods. Imaging is via multi-detector row CT and protocols include careful control of lung volume during scanning. Characterization includes not only anatomic-based measures but also functional measures including regional parameters derived from measures of pulmonary blood flow and ventilation. Image processing includes the automated detection of the lungs, lobes, and airways. The airways provide the road map to the lung parenchyma. Software automatically detects the airways, the airway centerlines, and the branch points, and then automatically labels the airway tree segments with a standardized set of labels, allowing for intersubject as well intrasubject comparisons across time. By warping all lungs to a common atlas, the atlas provides the range of normality for the various parameters provided by CT imaging.

Results. Imaged density and textural changes mark underlying structural changes at the most peripheral regions of the lung. Additionally, texture-based alterations in the parameters of blood flow may provide early evidence of pathologic processes. Imaging of stable xenon gas provides a regional measure of ventilation which, when coupled with measures of flow, provide for a textural analysis regional of ventilation-perfusion matching.

Conclusion. With the improved resolution and speed of CT imaging, the patchy nature of regional parenchymal pathology can be imaged as texture of structure and function. With careful control of imaging protocols and the use of objective image analysis methods it is possible to provide site-independent tools for the assessment of interstitial lung disease. There remains a need to validate these methods, which requires interdisciplinary and cross-institutional efforts to gather appropriate data bases of images along with a consensus on appropriate ground truths associated with the images. Furthermore, there is the growing need for scanner manufacturers to focus on not just visually pleasing images, but on quantitatifiably accurate images.

Key Words. Quantitative CT; airways; parenchyma; emphysema; interstitial lung disease; computer analysis; blood flow; ventitation.

Acad Radiol 2003; 10:1104–1118

[1] From the Departments of Radiology, (E.A.H., J.G., H.S., K.C.B) Biomedical Engineering, (E.A.H., J.M.R., O.S., D.C., G.M.) Electrical and Computer Engineering, (M.S., J.T., K.P.) and Medicine, University of Iowa, Iowa City, IA (S.S., G.M.); and the Department of Anesthesiology, The Johns Hopkins University, Baltimore MD (B.A.S.). Received June 6, 2003; revision requested June 26; revision received and accepted ____ . Supported in part by National Institutes of Health grants R01-HL060158 and R01-HL064368 (a Bioengineering Research Partnership). **Address correspondence to** E.A.H.

doi:10.1016/S1076-6332(03)00330-1

There is currently considerable interest in developing methods for quantitative imaging of the lung to identify disease early and to follow disease progression or to evaluate the result of interventions. There is a hope that imaging will accelerate drug discovery processes and that quantitative measures based on lung imaging will provide surrogate markers that have enhanced sensitivity and specificity relative to more conventional pulmonary function tests or other more subjective clinical parameters and thus accelerate the evaluation of disease interventions. The first report from the National Emphysema Treatment Trial (1), following the closure of patient enrolment, showed that radiologists reported information from computed tomography (CT) scans regarding relative distribution of emphysema emerged as one of only two of the primary evaluation parameters, defined at the study onset, that were found to be predictive of a successful surgical outcome. Computer-based quantitation of the lung is still under evaluation because this was entered into the study mid-course. Despite the importance of the radiologist's interpretation, there is increasing recognition that the human observer, unaided by computer-based image evaluation tools, is poorly reproducible in quantitating extent of disease or even in disease discrimination without relying on non–image-based patient history entries in the patient record (2). The need for improving the ability to detect and quantify lung pathology via computer-based image processing tools is reflected in a number of National Institute of Health-based initiatives seeking to gather ground truth databases associated with image data sets so that the process of developing and validating computer methodologies can be accelerated. Detection and characterization of lung nodules is an important example (3) with the National Lung Screening Trial (4) under way. Detection and characterization of interstitial lung disease (ILD) with the inclusion of emphysema has been recently identified as important, through a specific request from the National Institute of Health to establish a National Lung Tissue Research Consortium with an associated Radiology Center (NHLBI RFP HR 04-01) coordinating the gathering of volumetric CT data sets. The CT images, if gathered under carefully controlled protocols, will allow for cross-correlation of pathology and radiographic-based data and will begin to allow for the direct correlation of image density and texture (regional gray scale patterns) with pathologic findings. In this article, we will focus on image-based methodologies that our laboratory has developed to address the need for quantitating interstitial pathologies and for following lung regions of interest over time.

INTERSTITIAL LUNG DISEASES

Interstitial lung diseases are a complex grouping of disorders that affect the lung parenchyma and lead to respiratory failure if the cause is not removed or if therapy fails. Interstitial lung diseases may be loosely and simply classified into those associated with an acute inflammatory response predominantly mediated by neutrophils (a common example is adult respiratory distress syndrome); those that have a subacute/chronic inflammatory response predominantly mediated through lymphocytes (common examples are extrinsic allergic alveolitis or sarcoidosis), with or without granuloma formation; and those that have a chronic inflammatory response predominantly mediated by monocytes or macrophages (common examples are nonspecific interstitial pneumonia and emphysema). Additionally, there are other ILDs where the predominant abnormality is excessive fibrosis with minor inflammation, suggesting a defect in the fibroblast cellular control. Early CT quantification of pulmonary fibrosis and emphysema has been based on identifying those CT voxels in the lung field falling outside of an empirically derived Houndsfield Unit (attenuation) threshold (5–7).

There is a large list of known causes of ILDs, including inhaled organic and inorganic dusts, including cigarette smoke. However, there is also a large group of idiopathic interstitial disorders that have become increasingly well understood over the last decade. The etiology of these disorders remains unknown, although there is often some link to cigarette smoking. The notion that we and others have previously described (8), that the responses to cigarette smoking can either be an inflammatory response with fibrosis or an inflammatory response with lung destruction and emphysema formation, is probably too simple an explanation. The notion that inflammation leading to pulmonary fibrosis is a very good one was recently rearticulated and clearly discussed and now significantly revised (9). There is increased understanding now that emphysema, while usually characterized as an obstructive airway disease, is increasingly primarily an ILD with the airflow limitation being a secondary, yet very important event.

The idiopathic interstitial pneumonias can be classified into five pathologically distinct categories: usual intersti-

tial pneumonia (9–11); desquamative interstitial pneumonia (12); acute interstitial pneumonia (13); nonspecific interstitial pneumonia (14); and cryptogenic organizing pneumonia/bronchiolitis obliterans organizing pneumonia (15).

Research into these diseases is currently driven by the pathologic reclassification, now shown to be associated with different clinical outcomes. This splitting of what was formerly called "idiopathic pulmonary fibrosis" into the five major categories above has been a significant advance in the understanding of these disorders. This has allowed different theories of pathogenesis as well as different approaches to therapy based on the perceived therapeutic target (16). For instance, some therapies are now being directed not at anti-inflammatory measures, such as corticosteroids and methotrexate or azathioprine, but at fibroblast proliferation and reactivity. It is increasingly very important to correlate the CT changes of the lung parenchyma with the histopathology, and therefore extremely important that lung samples are taken from representative areas described by CT appearances.

The extent of disease on high-resolution CT certainly correlates with fibrosis on biopsy, as well as with physiologic impairment in these disorders. The CT scan has been used to direct the surgeon to biopsy specific abnormal regions of the lung under either thorascopic conditions or open thoracotomy (17), but often, because of the clinical features and CT findings, lung biopsy may not be needed (18).

Each of the subsets of the family of idiopathic interstitial pneumonias has a different natural history and outcome with current therapy. For idiopathic pulmonary fibrosis, the median survival is less than 3 years, with current therapies not changing the rapid decline in pulmonary function and the onset of pulmonary hypertension and cor pulmonale.

Chronic obstructive pulmonary diseases (COPD) are a family of diseases that include chronic bronchitis, emphysema, bronchiectasis, and chronic asthma. They are also frequently associated with cigarette smoking, either as a cause or as a major exacerbating factor. There is a large amount of literature on COPD, from new animal models (19) to community guidelines for home oxygen therapy and safety of procedures (20). The elastase/antielastase hypothesis still has interest in the pathogenesis and possible therapy in these disorders, but increasingly there is also interest in the notion of the "sick" fibroblast, with underactivity, as well as interest in the various polymorphisms of elastin. Therapy currently remains supportive. Of interest, and not unexpected given the common role of cigarette smoking in many of these disorders, is that the idiopathic interstitial pneumonias may frequently co-exist with the chronic obstructive airway diseases, especially emphysema.

Emphysema is defined as a condition of the lung characterized by abnormal, permanent enlargement of air spaces distal to the terminal bronchiole, accompanied by the destruction of their walls and without obvious fibrosis. Destruction in emphysema is defined as non-uniformity in the pattern of respiratory air space enlargement so that the orderly appearance of the acinus and its components is disturbed and may be lost. Emphysema has historically been identified and classified according to the macroscopic architecture of the removed, inflated, and fixed at a standard-pressure whole lung. Such patterns of destruction are clearly a target for objective tissue characterization methodologies using high-resolution CT imaging. Quantitative approaches to date have used only first-order measures and have largely been limited to mean lung density and assessment of the location of the lower fifth percentile cut-off on the lung density histogram (plotting number of pixels vs Houndsfield unit) (6,7,21–32).

Recently, there has been increased focus on not only the parenchyma but also the airways in emphysema patients. Coxson et al (33) have presented early evidence that suggest that there may be a familial basis for airway wall thickening in some patient groups with COPD. These early reports have not used careful control of lung volume during scanning protocols, and the data has not been evaluated volumetrically. Thus, it is not known if the observed changes in airway wall thickness are because of real wall thickening or the evaluation of varying airway generations with shifting cross sectional areas. It will be desirable to implement careful methods of assuring scanning at well-controlled lung volumes (either percent of vital capacity or at a given airway pressure).

Computed tomography provides an opportunity for evaluating the lung parenchyma and the bronchial tree, both structurally and functionally, in a cross-sectional and longitudinal study design, using the human observer, or more recently computer-assisted classification methods. However, relational databases of the complex CT findings with the lung pathology have not been available to ask fundamental questions that might also require lung tissue for ground truth.

QUANTITATIVE COMPUTED TOMOGRAPHY APPROACHES

Volumetric CT is accurate in determining lung volumes (34) and regional lung density (35,36). The primary steps in evaluating the lung, particularly for the purposes of detecting and following ILDs include:

1. Segmentation (identification of regional boundaries) of the lungs, lobes, and airways;
2. Identifying the airway center lines and thus branch points to match lungs across volumes and over time;
3. Automatically label airway segments to allow for the matching of subjects to a normative atlas;
4. Categorize lung field voxels according to their attenuation values (Houndsfield Units) and according to their place within the lung attenuation histogram;
5. Categorize lung regions according to texture-based attributes;
6. Categorize lung regions according to functional parameters such as ventilation and perfusion and according to the regional "texture" of the functional parameters.

IDENTIFICATION OF LUNG COMPONENTS ("SEGMENTATION")

Lungs

Automated segmentation of the lungs from a three-dimensional (3D) set of CT images is a crucial first step in the quantitative analysis of pulmonary physiology or pathophysiology. With large 3D image volumes becoming commonplace, routine manual segmentation to identify regions of interest is too cumbersome and time-consuming. In addition, manual analysis has significant inter-observer and intra-observer variability.

We have developed and validated a segmentation method to accurately extract the lungs from CT images (37) (see Fig 1). This approach, which can be used automatically or semi-automatically, relies on thresholding to obtain approximate initial lung masks. These lung masks are refined using topologic analysis (to delete cavities and small disconnected pieces, for example) and specialized processing to enforce anatomic constraints (such as using a graph search to find the most likely location of the line separating the left and right lung). Experimental studies using images acquired from humans have shown our method to be very accurate: computer-generated and manually defined lung areas (in pixels) correlated very well in individual slices ($r = 0.99$, $y = 1.01 \times -1{,}162$).

Figure 1. Lung, lobe and airway segmentation. Right and left lungs are found along with major fissures. In this image, the right horizontal fissure is not identified because of thick slice imaging. This fissure is found readily if 1.5 mm thick sectioning is achieved at scanning time.

We have developed new algorithms that directly address the pulmonary arteries, are more robust in the presence of disease, and generate contours that more closely matched those defined by the human observer. In the case of pneumonia, the pixels in a region with pneumonia are segmented into the lung region, rather than the chest region, even though the region with pneumonia is characterized by an abnormally high x-ray attenuation coefficient.

Lobes

We have developed a semi-automatic method for identifying the fissures in CT images (38) (Fig 1). Our method uses a combination of anatomic features and CT image features to identify the fissures on two-dimensional transverse slices. These features are combined into a cost function that reflects the likelihood that a pixel lies on the fissure. A graph search, which is a heuristic cost-based search technique, is used to find a path between the endpoints. Graph searching finds the minimum cost path between the two endpoints, where the cost function definition reflects the problem of interest. The user must initialize the process once for each fissure of interest, but once the procedure has been initialized the entire 3D surface

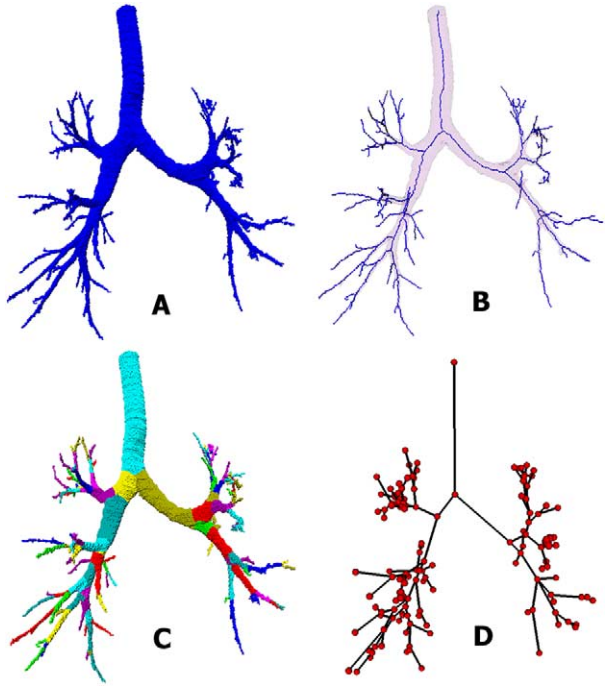

Figure 2. (**a**) Adaptive region growing-based airway segmentation; (**b**) Extraction of centerlines-topologically and geometrically correct thinning; (**c**) Partitioning segmented tree via isotropic label propagation; (**d**) Mathematical graph representation of the individual tree. The tree shown in **d** is stored in an XML file, which provides associated measures for each part of the tree. These measures include segment length, branch angles, regional lumenal area, wall thickness, segment luminal volume, segment surface area, regional minimum diameter, and the diameter of the orthogonal as well as regional maximum diameter.

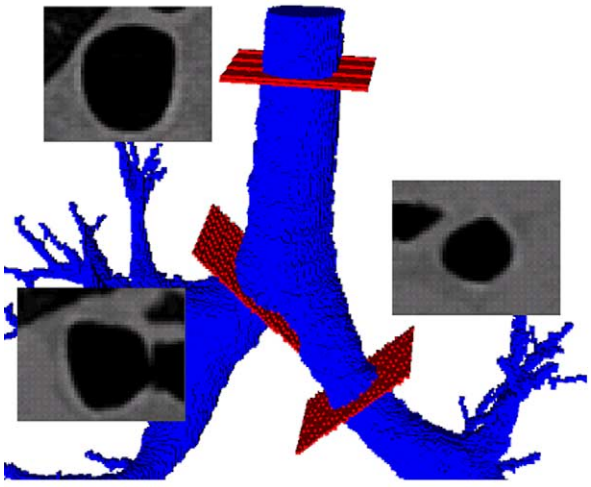

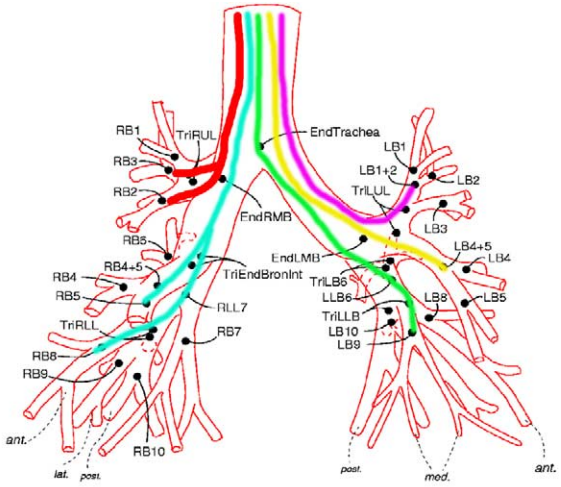

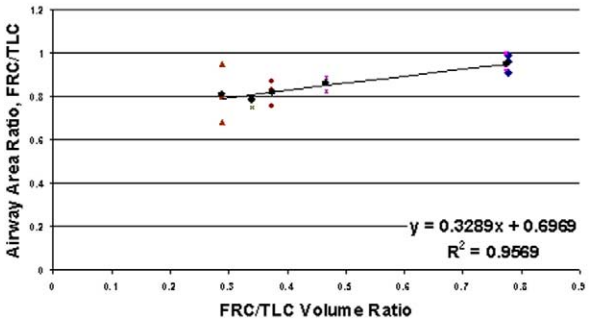

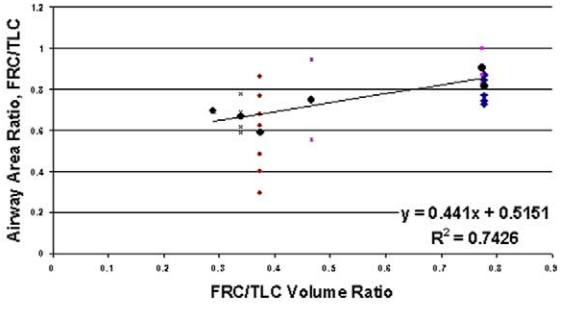

can be automatically identified. The overall root mean squared (RMS) error between manual tracing of the fissure and our semi-automatic method is about 2 pixels. Under development are methods to automatically initiate the lobe segmentation process through the development of a standard lung atlas representing the average shape of the normal human lung. The individual is then matched to the atlas and the location of the fissures in the atlas serve as the initial guess for the search initiation. More recent work from the laboratory has used an anatomic pulmonary atlas with a priori knowledge about lobar fissure shapes from a set of presegmented training data sets to achieve a fully automatic lobe segmentation (39).

Airway Lumen and Walls

The borders of the inner and outer airway walls have been detected to subvoxel resolution (40). Airways of interest range in size from 1–15 mm inside diameter. The small airways have very thin walls, typically on the order of 10%–15% of the inner diameter. The established full width at half-maximum method for measurement can give very inaccurate results for these small, thin-walled structures. To address this problem, we use a new method of estimating the airway wall locations. We first assess the point spread function of the particular scanner/slice selection/reconstruction algorithm of interest and then use a model-based deconvolution to account for blur introduced in the scanning process. This is more accurate than existing wall detection methods, especially for thin-walled structures. Phantom studies show the new method to be applicable across a wide variety of airway sizes (40,41).

Fully Automated Segmentation, Skeletonization, and Branchpoint Matching in Human Airway Trees

As part of our efforts to use the airways as a roadmap to the lung, we recently developed a system outlined by the steps shown in Figure 2 (42,43).

Main System

The developed system consists of three main blocks: airway tree segmentation (Fig 1A), skeletonization (Fig 1B), and branchpoint localization (Fig 1D), and segment identification (Fig 1C) along with branchpoint matching.

Airway Tree Segmentation

The airway segmentation uses a seeded region growing, starting from an automatically identified seedpoint within the trachea. The algorithm is designed so that it can overcome subtle gray level changes (eg, beam-hardening). On the other hand a "leaking" into the surrounding lung tissue can be avoided. The implementation of the algorithm uses graph algorithms that make it fast and memory-friendly. The method reliably segments the first five to six airway generations.

Skeletonization and Branchpoint Localization

The binary airway tree formed in the previous step is skeletonized to identify the 3D center lines of individual branches and to determine the branchpoint locations. A sequential 3D thinning algorithm reported by Palágyi et al (43) was customized for our application. False branches are pruned, and the resulting skeleton is guaranteed to lie in the middle of the cylindrically shaped airway segments. The automatically determined branchpoint positions match very well with the positions determined by human experts. The overall quality of the skeletonization output is exceptionally high (compared with published results from other groups). The complete skeletonization process executes in a very short time (less than 50 seconds for a $512 \times 512 \times 550$ voxel volume, measured on standard PC hardware).

Branchpoint Matching

The goal of branchpoint matching is to find anatomically corresponding branchpoints in two different airway trees. The output from the skeletonization process is rep-

Figure 3. Regional airway geometric parameters are calculated from 3D images along planes selected to be perpendicular to the regional airway long axis. After automatically applying a naming template to the extracted airway tree, we mapped out the area changes in response to lung volume changes. As a sample set of measures from such an analysis, we graphed the percent change in airway cross-sectional area as a function of fractional lung volume change relative to total lung capacity for seven paths within the bronchial trees of six normal volunteers. The lower left panel represents airways with a total lung capacity cross-sectional area between 250 and 450 mm^2 and the lower right panel represents airways with a total lung capacity cross-sectional area between 25 and 50 mm^2. Note the increased dispensability of the steeper slope of the smaller airway segments. Because both airways and parenchymal alter their anatomic properties considerably with lung volume, it is important to image the lung at standardized lung volumes if one is to reach meaningful conclusions from quantitative measures derived from the CT images. FRC, functional residual capacity, TLC, total lung capacity.

resented as a mathematical tree, and graph algorithms are applied that match corresponding branchpoints. The algorithm executes in less than 2 seconds when matching two trees with 150–200 branchpoints each (measured on standard PC hardware). An evaluation using phantom data as well as in vivo scans showed a high agreement between the automatically obtained matches and matches provided by human experts (between 85% and 97% agreement between computer-determined vs independent standard, less than 1% wrong matches).

Methods have been established to automatically label the airway tree with a nomenclature that we have established which takes into account the most common variability between individuals. This nomenclature (shown in Fig 3) can be applied to images of multiple lung volumes of the same individual to allow us to track the change in airway dimensions along an airway path as well as the change in airway dimensions with change in lung volume. Our airway segmentation methods have been shown to be robust in the presence of significant emphysema and when applied to images acquired using low-dose scanning protocols. The changes in airway area as a function of fractional changes in lung volume along seven major paths leading to the individual lung lobes are shown in Figure 4 (44).

DYNAMIC VERSUS STATIC IMAGING

Because respiration is a dynamic process, and many pathologic conditions of the lungs are based on processes that are altered only during active breathing (such as frequency dependence of compliance, dynamic compression of the airways, and so on) and because many of the very people whom one might wish to image are the very people who have difficulty with breath holding, even for short periods of time, there is considerable interest in capturing the complete lung volume at multiple points within the respiratory cycle during active respiration.

Respiratory Gating and Lung Volume Control

Methods have emerged which allow for the retrospective reconstruction of a spirally collected data set of the heart if the electrocardiogram has been simultaneously recorded with the raw projection data. However, because respiration is considerably slower than the heart beat, and because the respiratory cycle is not as repeatable from breath to breath, the retrospective method is not very practical for the lung. Therefore, we have devised a method to scan the lung axially and to gate the image acquisition to fixed volumetric locations within the respiratory cycle. With a four-slice multi-detector row CT (MDCT) scanner, we have scanned the lung at two points within the respiratory cycle while moving the table location by the combined thickness of two of the four slices between each gated scan acquisition. This process is repeated for the same two volume locations within sequential respiratory cycles until one has imaged the full extent of the lung.

It is common to monitor airflow at the mouth and lung volumes within any standard pulmonary function laboratory. However, the accuracy required by the above described respiratory-gated image acquisition requires much tighter tolerances and is much more demanding than most pulmonary function testing equipment. We continue to test the various approaches to following lung volumes accurately for the purposes of gating slice acquisitions. Methods include the use of mouth-based air flow methods including a pneumotachometer, ultrasound probe, or a turbine, and a chest-wall–based inductance plethysmograph (Respitrace, North Bay Village, FL). The images in

Figure 4. By use of a pneumotachometer or other lung volume-tracking device (left panel) we are able to follow respiration and to gate axial scans to specific points within the respiratory cycle. Using a MDCT, a set of axial sections are obtained at multiple points within a respiratory cycle and then the table is advanced to acquire the adjacent set of slices at the same lung volumes of the next respiratory cycle. The right panel of this image shows a volume rendering of the 3D lung and a coronal section sampled from the center of the stacked image data set. Note that every four slices used to produce these 3D images were from a different respiratory cycle than the adjacent four slices and yet anatomy is depicted as being continuous from apex to base of the lung.

Figure 5. Assessment of the lung parenchyma based on the lung density (attenuation) histogram. (**Upper left panel**) Density histogram; (**upper middle panel**) Accumulation histogram; (**upper right panel**) Quantitative report based on the lung density evaluation. (**Middle row**) Coronal, transverse, and sagittal sections of volumetric CT image of the chest with a color overlay showing the location of the voxels falling below the selected threshold (yellow vertical line in the upper row graphs). Also shown are the regions automatically selected for the core and rind measurements. In these images the lungs are also divided into thirds based on the apical to basal distance measure. With thinner section scanning, the lung can be divided into actual lobes. (**Lower row**) Three views of a volume rendering of the lung with the distribution of voxels falling below the selected threshold depicted in green.

Figure 6. Characterization of regional lung parenchyma based on the adaptive multiple feature method (AMFM).

Figure 4.

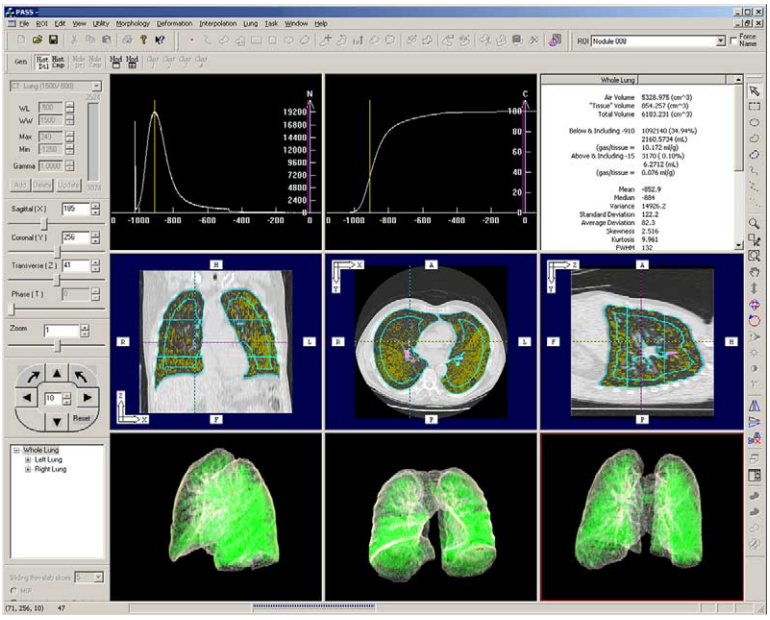

Figure 5.

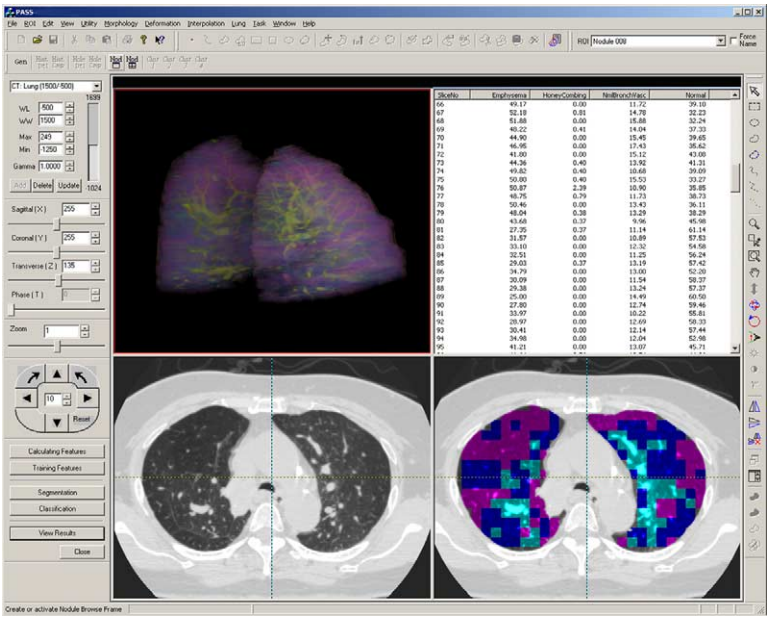

Figure 6.

Figure 4 show a subject lying within the MDCT scanner breathing quietly in preparation for scanning. In this case, the subject is breathing through a pneumotachometer. The images to the right show a volume rendering and a coronal section of the resulting volumetric image of the lungs calculated from the stacked set of axial images. Note that every four axial slices used to generate these images were gathered during sequential respiratory cycles and yet all anatomic structures from base to apex of the lungs are well aligned demonstrating the ability to very accurately track lung volumes over short time frames. In the configuration shown on the left of Figure 4, there is a mouth piece with an associated high-frequency balloon valve that can be occluded during scanning such that the subject's lung volume is held at a fixed percent of the vital capacity. Alternatively, the subject can relax against various levels of positive end expiratory pressure and scanning occurs during prolonged expiratory pauses. We have recently completed a study in which we have compared multiple methods of lung volume monitoring and image acquisition (41).

PARENCHYMAL ANATOMY

Regional Lung Air Content

With the grey scale of a CT image calibrated such that air is −1,000 and water is 0, blood is approximately 45, and dense bone is +1,000, it is possible to calculate the amount of air and "tissue" (tissue in this context includes blood volume) in each voxel (35). If one is able to follow the motion of a specific location in the lung through multiple points in a respiratory cycle, and one can identify a specific anatomic volume through the cycle, it becomes possible to measure change in local air content and thus regional specific ventilation. It is critical to assure that scanners remain within appropriate calibration specifications, and it is our recommendation that purpose-built phantoms be used on a regular basis to verify the accuracy of the scanners. These phantoms must extend across the full range of densities between air and water.

Histogram-Based Analysis of Parenchymal Pathology

With the growing interest in quantitating peripheral lung disease, there is a need to develop objective measures of pathology, not just yes or no answers regarding the presence of disease. With the recognition that many peripheral pathologic processes either increase or decrease regional lung density, there has been a growing focus on quantitating the distribution of lung intensity values within CT images. This is commonly achieved through use of a histogram plot (shown in the upper left panel of Fig 5). Through largely empirical means, investigators have found that when the lung is scanned with volume held near total lung capacity and CT slice thickness set to be near 1cm, the emphysematous regions of the lung in patients with significant disease fall roughly below −910 Houndsfield Unit. When slice thicknesses are thinner, the cut-off value is closer to −950. Coxson et al (29) compared pathology measures of lung surface area versus in vivo CT images of the same lung and developed criteria for assessing the lung to be severe, moderate, and mild emphysema-like. The calibration is a linear transformation of the Houndsfield Unit values and thus is subject to the same variability as Houndsfield Unit values in regards to assigning surface area values and emphysema cut-offs relative to specific scan protocols. In addition to assigning cut-off values for emphysema, others have sought to identify the value at which one finds the lowest 15th percentile of the histogram plot of voxel intensities.

Changes in this value when following a group of subjects with emphysema also serve as an index of change over time. Figure 5 shows the software implementing this histogram approach to parenchymal assessment. One can visualize the distribution of regions assigned as being within the emphysematous range either as orthogonal cross sections or within the context of 3D lung displays. By dividing the lung into either thirds or actual lobes, inner core, outer rind, etc, one can further characterize the amount and extent of these emphysematous regions. We have validated our software in three ways:

1. We replaced the voxel values within the lung fields of a series of subjects with a known random set of values from a look-up table and verified that the know distribution of numbers are returned when the images are sent through our analysis software.
2. We recently compared our analysis versus the analysis of Coxson et al for the same group of 14 emphysema patients. Measures of percent emphysema obtained by the two software packages match to within a fraction of 1% of each other (45).
3. We have had three different image analysis technicians with experience varying from 10 years to 1 week analyze 20 lung data sets three times each, and the intra and inter subject variability in percent emphysema scores and total lung air and tissue measures differed by less than 1% of each other.

Because early evidence in the literature suggests that the distribution of emphysematous like voxels in the "rind" versus the "core" of the lung may be predictive of surgical outcomes for lung volume reduction surgery (21), we have implemented a 3D version of a core-rind algorithm which allows the user to identify the thickness of the rind, and includes within the core that portion of the lung that is contiguous with the mediastinum encompassing the extra-pulmonary airways, veins, and arteries.

Parenchymal Texture

While the histogram-based method of lung parenchymal assessment has proven to be highly useful in building quantitative tools for assessing patients with moderate to severe emphysema, simple histogram-based methods are unsatisfactory for mild disease, and when there is mixed pathologic processes present. To address this, we have made significant advances in the use of tissue characterization to classify parenchymal patterns in reconstructed CT data sets (46–48).

A texture-based computer-assisted method, called the Adaptive Multiple Feature Method (AMFM), has been developed and involves three steps: (a) feature extraction from the region of interest; (b) optimal feature selection based on a training set; and (c) classification of the test set. The AMFM uses mathematical formulations of the bright/dark pattern within the lung field to establish "feature" sets. These features include first order measures based on density histograms such as mean lung density, kurtosis, and skewness, but also uses higher order measures including entropy, run-length encoding, and stochastic fractal dimensions. Training and test sets are established by having panels of experts reach consensus regarding regional image classifications such as nodular, ground glass, broncho-vascular, emphysema-like, and normal. Using a Bayesian classifier, the AMFM is then trained to identify the best subset of features that will separate one tissue type from another or simultaneously separate multiple tissue types.

Three studies using the AMFM have been reported to date that show the power of such an approach in separating multiple simultaneous tissue types (46–48). In the first study, we sought to simply differentiate disease types globally. However, radiologists do not tend to simply diagnose diseases, but rather evaluate regional appearances of the lung field and then, based on the pattern of pathology along with the patient history, an evaluation of the image is reported. In the second experiment, a 31×31 pixel window stepped across the lung field was used to classify regions of tissue. Fifteen features were selected by AMFM for this window size. In a study comparing five observers' ability to classify the same 31×31 pixel lung regions as the computer, three repeat readings were obtained; two with the observers blinded to the patient's diagnosis and supporting clinical materials and in a third reading the observers were given full access to the patient's clinical records and the final pathology reports when available. In all cases, the within and between observer agreement amongst themselves and with the computer were on the order of 35%–60%. The computer agreed with itself 100% of the time. On the third reading when the observers (well-trained radiologists and pulmonologists) were given access to the clinical records, in all cases, the observers significantly increased their agreement with the computer (48).

In further studies, using the AMFM approach, we sought a means of identifying an index of our sensitivity to early parenchymal pathology (2). This is of particular challenge because of the lack of gold standards. We obtained a unique CT data set from Dr Paul Enright, gathered as part of a National Institute of Health Lung Special Center of Research (SCOR) carried out at the University of Arizona (Tucson, Arizona). Data divided into three groups: never-smokers with normal pulmonary function tests (NONSMK); smokers with normal pulmonary function tests (SMK); and smokers with COPD (COPD). We sought to determine if the AMFM would be able to differentiate between "normal" regions selected from normal nonsmokers and those selected from the COPD subjects.

Discrimination Between Traced "Normal" Regions

To test this premise, we performed regional classification studies where example regions of normal lung from NONSMK subjects (NN) were outlined along with example regions of emphysema lung from COPD subjects (EC), "normal appearing" lung from COPD subjects (NC), and mild emphysema lung from COPD subjects (MC). The regions were outlined by an experienced pulmonologist and physiologist. The AMFM was trained to differentiate these groups using half of the 31×31 pixel block samples from these regions, and it was tested on the remaining half. The purpose of this experiment was to determine (a) if these groups could be successfully differentiated, and (b) if so, then what percent of a NONSMK lung, a SMK lung, and a COPD lung fell into each of these groups. These four groups were differentiated with an overall accuracy of 85.3%, showing that the four

groups could be discriminated successfully using our tissue characterization technique. Of importance is the fact that normal-looking lung from NONSMK subjects is indeed different from what appears to be normal in COPD subjects. The differences may be so subtle that they are not apparent to the human eye. An example of display methods used to visualize patterns of tissue classifications is shown in the right panel of Figure 6.

Hole Size

Recently, Mishima et al (49) have put forward the notion that, if the destruction of lung parenchyma in emphysema is initially a random process and then later is governed by the notion that the presence of small "holes" increase the likelihood of further destruction to occur in that lung region, thus causing small holes to join to form larger holes, the initial hole distribution, when plotting holes versus hole size on a log-log plot should provide a linear relationship and then the process of small holes joining to form larger holes should progressively alter the slope of the log-log relationship. We have implemented such an analysis within our Pulmonary Analysis Software Suite, as seen in Figure 7. Note that all the holes falling below a given size are plotted in yellow and all of the larger holes (interactively selected on the log-log plot) are mapped in green on the CT images. It is striking, and of interest, that the color overlay, identifying the larger holes in the patient shown in Figure 7, is so tightly limited to the lower lobe that the color overlay provides a clear demarcation of the lobar fissure.

FUNCTIONAL IMAGING

Perfusion

In addition to imaging structure and dynamic changes in structure and associated changes in regional air content, it is also possible to begin to use sub-second MDCT to assess regional ventilation and perfusion as a means of additional features for characterizing regional lung pathology. Perfusion is measured by injecting iodinated contrast agent as a bolus and to then axially image (nonspiral mode where table sets in a fixed location during scanning) during a breath hold with the scanner gated to the same point in each cardiac cycle. Regional perfusion quantitation assumes that the height of the curve is a measure of the flow within that tissue regions of interest (50–54). This is based on a standard indicator dilution model with the additional assumption that the entire indicator resides within the regions of interest for a finite period of time before exiting. This then allows analysis to proceed similarly to standard microsphere methods.

Subvoxel Resolution of Perfusion and Kinetic Parameters to Evaluate Microvascular Physiology

With the concern that time-attenuation curves (because of bolus transit) obtained from voxels in the lung parenchyma do not represent flow solely at the air/blood interface, but may also represent flow in small arteries (partial volume effect). We sought a method to separate the arterial and capillary bed time-attenuation curves on a voxel by voxel basis. Our early efforts used an fast Fourier transform (FFT)-based deconvolution algorithm to recover regional residue functions that describe the inherent regional pulmonary vascular transport characteristics (ie, distribution of tracer particle residence times, hence transit times, within the regional vascular bed).

Deconvolution of the pulmonary artery and regional parenchymal time-attenuation curves consistently yield bimodal regional residue functions consisting of a sharp, narrow peak and a second, overlapping more dispersed curve component. By separating out the first sharp, narrow curve component from the second more dispersed component and re-convolving the second component with the original arterial curve, we are able to derive a new parenchymal curve which more closely reflects the micro vascular blood flow parameters.

Findings to date (54) support our notion that we are able to recover both microvascular and arterial curves within a peripheral regions of interest. The ability to image regional distribution of micro vascular transit times is of considerable interest, in part, because we hypothesize that a disruption of the normal local patterns of this measure may indicate early inflammatory processes whereby there is a margination of neutrophils and a thickening of arteriolar walls, both of which might be expected to alter mean transit times in the micro vascular bed (55).

Ventilation

The measurement of lung ventilation, lung volume, and tidal volume has traditionally been made for the entire lung, despite the fact that lung function in both health and disease is inhomogeneous. Xenon-enhanced CT is a method for the noninvasive measurement of regional pulmonary ventilation, determined from the wash-in and/or wash-out rates of the radio dense, nonradioactive gas xenon as measured in serial CT scans. While the prospect of measuring regional ventilation with stable xenon has been established for many years (56,57), advances in CT

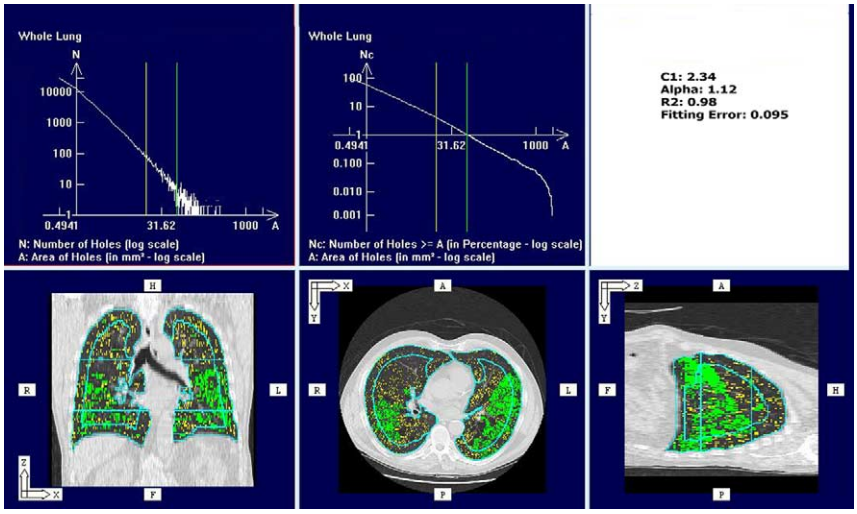

Figure 7. Evaluation of the distribution of holes within the lung where holes are defined by contiguous voxels in two or three dimensions with an x-ray attenuation falling below a given threshold. The upper left graph plots log of hole area on the x-axis and number of holes on the y-axis. The middle graph in the upper row plots percentage of holes rather than absolute number of holes on the y-axis. An upper and lower threshold is set by the green and yellow lines on the graphs, respectively, and the location of the large (green) and small (yellow) holes are color coded onto the coronal, transverse, and sagittal images, respectively, in the lower row. The slope of the log-log graph data in the middle panel of the upper row is displayed in the upper right panel. The slope of the relationship is given as Alpha and the goodness of fit is given as R^2.

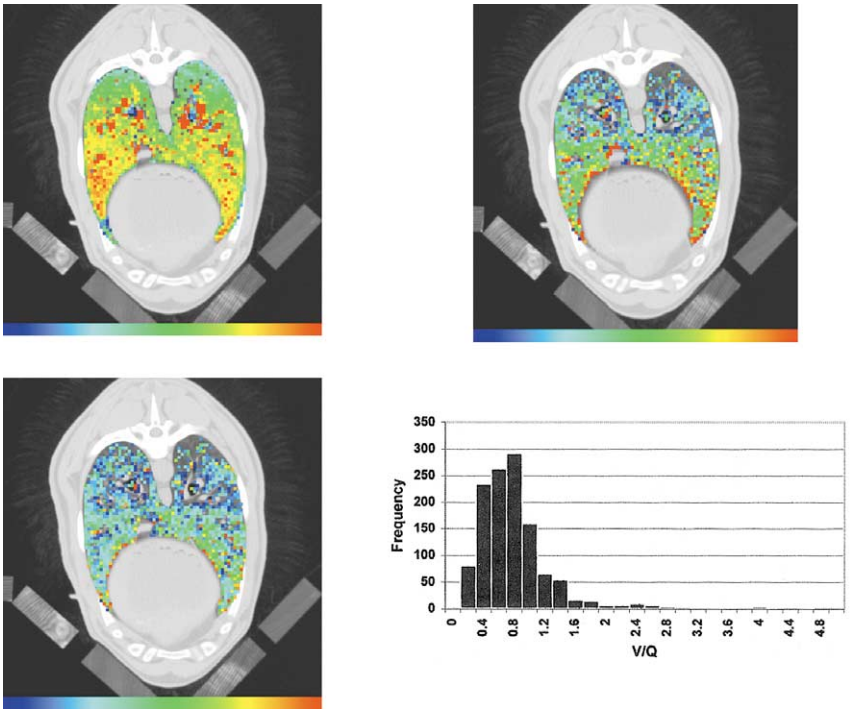

Figure 8. Prone anesthetized sheep imaged at functional residual capacity during a breath-hold for perfusion and at end expiration for ventilation measures. The upper left panel represents a color map of raw blood flow. The upper right panel represents a color map of raw ventilation calculated for a xenon wash-in protocol. Both the blood flow and ventilation color scales range from 0 to 0.06 mL/min. Note that neither blood flow nor ventilation are normalized here to regional voxel parenchymal content. The normalization, which is important for the evaluation of etiher parameter alone and is routinely calculated as part of our studies, is not necessary here because the goal is a ventilation/perfusion (V/Q) map, where both V and Q normalization values cancel. The lower left panel shows a map of V/Q with the color scale set to range between 0 and 2. The software performs a rigid body rotation and translation to identify the optimal match between the V and Q scans. Once the MDCT scanners begin to broaden the cone beam to allow for larger Z-axis coverage in the axial scanning mode, we will be able to perform 3D warping of the datasets based on the airway and vascular branch points and the lobar surfaces. Note that while there is a ventral heterogeneity in regional ventilation and perfusion, the matching of the two measures takes on a greater homogeneity than is seen in either of the independent parameters, indicating that physiologic and physical mechanisms are at work to assure regional matching of V and Q. The lower right panel shows a histogram plot where voxels of various V/Q ranges have been binned together. Note that in this example, the mode of the histogram plot is approximately 0.8, which is what standard respiratory textbooks report as being the standard normal, global V/Q relationship. While we believe that the absolute values of V, Q, and V/Q are of great interest, of likely greater value is the information embedded in the regional texture features of these measures as shown in Figure 9.

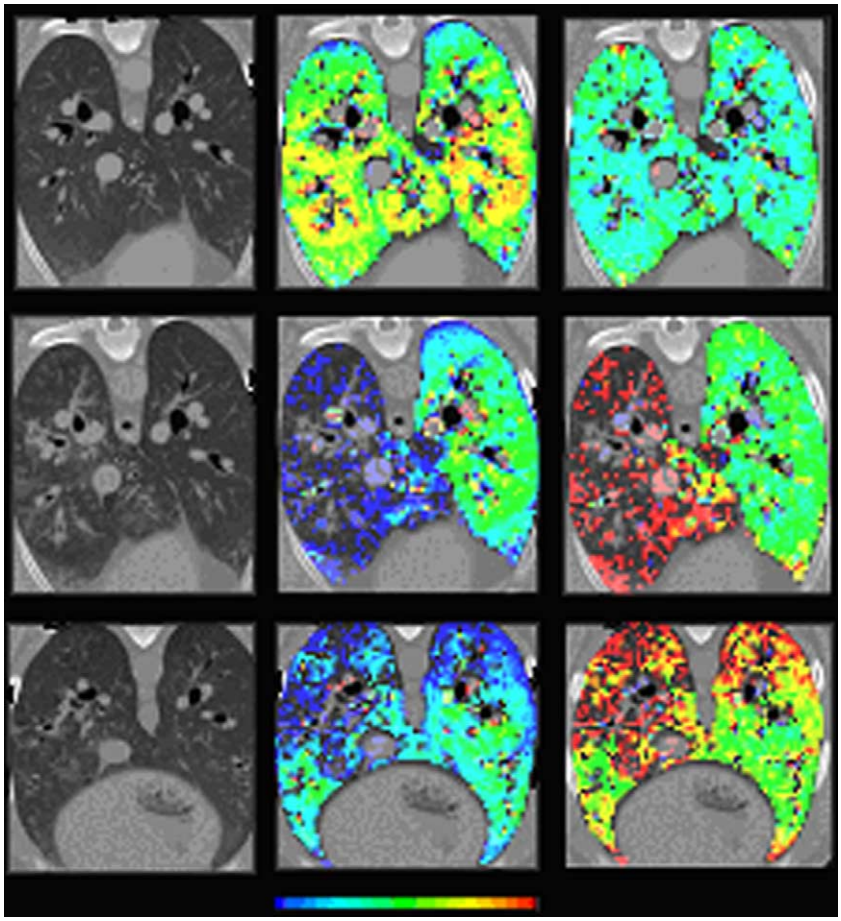

Figure 9. Blood flow (**middle column**) and mean transit time (**right column**) maps in a prone sheep followed through the time course before (**upper row**) and flowing administration of papain to the right lung (**middle row**) On day 16, note that while the visible evidence in the gray scale images (**left column**) has largely cleared, the blood flow maps remain as clear evidence of the presence of interstitial pathology. Also, note the unexpected finding of the involvement of the dorsal region of the left (untreated) lung. Color scales for the images (blue to red) are 4–12 mL/sec/g tissue and 3–7 seconds for pulmonary blood flow (PBF) and mean transit time, respectively.

technology have increased the speed and resolution of imaging studies and now make practical the application of this technique for physiologic and clinical studies.

Recently, the methods for xenon-enhanced CT to measure regional pulmonary ventilation have been updated (58–62). While monitoring respiration and gating axial scans (ie, 16 slices at a time on a 16-slice MDCT scanner) to a fixed lung volume during tidal breathing, an individual breathes a mixture of xenon gas and oxygen. The time-based regional attenuation changes in the lung associated with regional wash-in and/or wash-out of the xenon gas mixture provide the information needed to calculate regional time constants of gas turnover which, when combined with measures of the initial air volume of the lung region, provide measures of regional ventilation. Combined with the unique capability of CT to describe anatomic detail and regional pulmonary perfusion (53,54); CT, as a single imaging modality, can provide a complete noninvasive structural and functional characterization of the lung. With the development of high-speed, gated, volumetric image acquisition technology the xenon-enhanced CT method can now be further advanced to measure detailed ventilation distributions throughout the entire lung. The images in Figure 8 demonstrate a regional mapping of ventilation (V), perfusion (Q), and V/Q matching for an anesthetized sheep studied prone in a four-slice MDCT scanner. Slice thickness is 2.5mm, rotation time was 0.5 seconds. Exposures settings were 120 mAs and

90 kV. Note that the heterogeneity of V/Q is considerably less than that of the individual V and q measures, showing the close matching of the two physiologic parameters. The lower right panel of Figure 8 shows the number of voxels falling with bins of V/Q values with the mode falling at approximately 0.8, which is what one would expect for a normal lung based on reports in almost any respiratory physiology text book. Here, however, we have the region by region values, tied to anatomic detail rather than a single value describing global lung function.

Texture of Functional Parameters

While we have made significant advances in our ability to use anatomic texture to characterize the regional state of the lung, regional texture of functional parameters are expected to provide important signs of the early pathophysiologic processes that lead to parenchymal pathology. Figure 9 shows the changes in pulmonary blood flow and mean transit times in a sheep model of emphysema where papain is infused into the lung and then the lungs are studied over time (55). An unexpected observation was made in this animal: note that the inflammatory process is detected not only in the right lung that received the intended papain lavage, but also in the left dorsal lung region that clearly received an unintentional papaine exposure. This effect of papain on the left lung would have gone unnoticed had we been looking only at the lung density images.

CONCLUSIONS

With careful attention to the scanning protocols, including the lung volume at which one scans, it is now possible to establish a normative atlas of the human lung based on CT imaging and to use these normal values to detect pathologic processes related to the ILD. The quantitative measures reflect both the structural as well as functional attributes of the lung. There has been a common misperception that CT imaging is limited to the study of anatomic detail. While x-ray CT is the modality of choice for studying lung anatomy, it is also capable of providing significant functional information. There remains a critical need for establishing ground truth data against which the emerging quantitative CT data can be compared and calibrated, especially with the recent advances in the pathology and the cellular understanding of the ILDs.

REFERENCES

1. Fishman A, Martinez F, Naunheim K, et al. A randomized trial comparing lung-volume-reduction surgery with medical therapy for severe emphysema. N Engl J Med 2003; 348:2059–2073.
2. Uppaluri R, McLennan G, Enright P, Standen J, Boyer-Pfersdorf P, Hoffman EA. Adaptive Multiple Feature Method (AMFM) for the early detection of parenchymal pathology in smoking population. SPIE Med Imaging Physiol Function 1998; 3337:8–13.
3. Clarke LP, Croft BY, Staab E, Baker H, Sullivan DC. National Cancer Institute initiative: lung image database resource for imaging research. Acad Radiol 2001; 8:447–450.
4. Truong MT, Munden RF. Lung cancer screening. Curr Oncol Rep 2003; 5:309–312.
5. Rienmuller RK, Behr J, Kalender WA, et al. Standardized quantitative high resolution CT in lung diseases. J Comput Assist Tomogr 1991; 15:742–749.
6. Kalender WA, Fichte H, Bautz W, Skalej M. Semiautomatic evaluation procedures for quantitative CT of the lung. J Comput Assist Tomogr 1991; 15:248–255.
7. Kalender WA, Rienmuller R, Seissler W, Behr J, Welke M, Fichte H. Measurement of pulmonary parenchymal attenuation: use of spirometric gating with quantitative CT. Radiology 1990; 175:265–268.
8. Walsh RL, Dillon T, Scicchitano R, McLennan G. Heparin and heparin sulfate are inhibitors of human leukocyte elastase. Clin Sci 1991; 81: 341–346.
9. Gross TJ, Hunninghake GW. Idiopathic pulmonary fibrosis. N Engl J Med 2001; 345:517–525.
10. Katzenstein AL, Myers JL. Idiopathic pulmonary fibrosis: clinical relevance of pathologic classification. Am J Respir Crit Care Med 1998; 157:1301–1315.
11. Ryu JH, Colby TV, Hartman TE. Idiopathic pulmonary fibrosis: current concepts. Mayo Clin Proc 1998; 73:1085–1101.
12. Yousem SA, Colby TV, Gaensler EA. Respiratory bronchiolitis-associated interstitial lung disease and its relationship to desquamative interstitial pneumonia. Mayo Clin Proc 1989; 64:1373–1380.
13. Katzenstein AL, Myers JL, Mazur MT. Acute interstitial pneumonia. A clinicopathologic, ultrastructural, and cell kinetic study. Am J Surg Pathol 1986; 10:256–267.
14. Katzenstein AL, Fiorelli RF. Nonspecific interstitial pneumonia/fibrosis. Histologic features and clinical significance. Am J Surg Pathol 1994; 18:136–147.
15. Epler GR. Heterogeneity of bronchiolitis obliterans organizing pneumonia. Curr Opin Pulm Med 1998; 4:93–97.
16. Mason RJ, Schwarz MI, Hunninghake GW, Musson RA. NHLBI Workshop Summary. Pharmacological therapy for idiopathic pulmonary fibrosis. Past, present, and future. Am J Respir Crit Care Med 1999; 160:1771–1777.
17. Kazerooni EA, Martinez FJ, Flint A, et al. Thin-section CT obtained at 10-mm increments versus limited three-level thin-section CT for idiopathic pulmonary fibrosis: correlation with pathologic scoring. AJR Am J Roentgenol 1997; 169:977–183.
18. Raghu G, Mageto YN, Lockhart D, Schmidt RA, Wood DE, Godwin JD. The accuracy of the clinical diagnosis of new-onset idiopathic pulmonary fibrosis and other interstitial lung disease: a prospective study. Chest 1999; 116:1168–1174.
19. Wright JL, Churg A. Animal models of cigarette smoke-induced COPD. Chest 2002; 122(Suppl 6):301S–306S.
20. Hattotuwa K, Gamble EA, O'Shaughnessy T, Jeffery PK, Barnes NC. Safety of bronchoscopy, biopsy, and BAL in research patients with COPD. Chest 2002; 122:1909–1912.
21. Nakano Y, Coxson HO, Bosan S, et al. Core to rind distribution of severe emphysema predicts outcome of lung volume reduction surgery. Am J Respir Crit Care Med 2001; 164:2195–2199.
22. Diallo MH, Guenard H, Laurent F, Carles P, Giron J. Distribution of lung density and mass in patients with emphysema as assessed by quantitative analysis of CT. Chest 2000; 118:1566–575.
23. Madsen MT, Uppaluri R, Hoffman EA, McLennan G. Pulmonary CT image classification with evolutionary programming. Acad Radiol 1999; 6:736–741.

24. Nakano Y, Sakai H, Muro S, et al. Comparison of low attenuation areas on computed tomographic scans between inner and outer segments of the lung in patients with chronic obstructive pulmonary disease: incidence and contribution to lung function. Thorax 1999; 54: 384–389.
25. Bae KT, Slone RM, Gierada DS, Yusen RD, Cooper JD. Patients with emphysema: quantitative CT analysis before and after lung volume reduction surgery. Work in progress. Radiology 1997; 203:705–714.
26. Mishima M, Oku Y, Kawakami K, et al. Quantitative assessment of the spatial distribution of low attenuation areas on X-ray CT using texture analysis in patients with chronic pulmonary emphysema. Front Med Biol Eng 1997; 8:19–34.
27. Madani A, Keyzer C, Gevenois PA. Quantitative computed tomography assessment of lung structure and function in pulmonary emphysema. Eur Respir J 2001; 18:720–730.
28. Nishimura K, Murata K, Yamagishi M, et al. Comparison of different computed tomography scanning methods for quantifying emphysema. J Thorac Imaging 1998; 13:193–198.
29. Coxson HO, Rogers RM, Whittall KP, et al. A quantification of the lung surface area in emphysema using computed tomography. Am J Respir Crit Care Med 1999; 159:851–856.
30. Stolk J, Dirksen A, van der Lugt AA, et al. Repeatability of lung density measurements with low-dose computed tomography in subjects with alpha-1-antitrypsin deficiency-associated emphysema. Invest Radiol 2001; 36:648–651.
31. Zagers H, Vrooman HA, Aarts NJ, et al. Assessment of the progression of emphysema by quantitative analysis of spirometrically gated computed tomography images. Invest Radiol 1996; 31:761–767.
32. Reinmuller R, Behr J, Kalender WA. Standardized quantitative high resolution CT in lung diseases. J Comput Assist Tomogr 1991; 15:742–749.
33. Coxson H, Patel B, Nakano Y, et al. The role of emphysema and airway wall dimensions in chronic obstructive pulmonary disease (COPD). Am J Respir Crit Care Med 2003; 167:A81.
34. Hoffman EA, Sinak LJ, Robb RA, Ritman EL. Noninvasive quantitative imaging of shape and volume of lungs. J Appl Physiol 1983; 54:1414–1421.
35. Hoffman EA. Effect of body orientation on regional lung expansion: a computed tomographic approach. J Appl Physiol 1985; 59:468–480.
36. Hoffman EA, Ritman EL. Effect of body orientation on regional lung expansion in dog and sloth. J Appl Physiol 1985; 59:481–491.
37. Hu S, Hoffman EA, Reinhardt JM. Automatic lung segmentation for accurate quantitation of volumetric X-ray CT images. IEEE Trans Med Imaging 2001; 20:490–498.
38. Zhang L, Hoffman EA, Reinhardt JM. Lung lobar segmentation by graph search with 3D shape constraints. SPIE Med Imaging Physiol Function 2001; 4321:204–215.
39. Zhang L, Hoffman EA, Reinhardt JM. Atlas-driven lung lobe segmentation in volumetric x-ray CT images: 5031, 2003: 308–319.
40. Reinhardt JM, D'Souza ND, Hoffman EA. Accurate measurement of intra-thoracic airways. IEEE Trans Med Imaging 1997; 16:820–827.
41. Saba O, Beck K, Chon D, Nixon E, Hoffman E. Lung volume measurement reproducibility using gated-axial and spiral multi-row detector CT (MDCT). Am J Respir Crit Care Med 2003; 167:A844.
42. Tschirren J, Palagy K, Hoffman E, Beck K, McLennan G, Sonka M. Fully automated quantitative evaluation of human airway trees in volumetric multi-row detector CT data. Am J Respir Crit Care Med 2003; 167:A847.
43. Palagyi K, Tschirren J, Hoffman E, Beck K, Sonka M. Quantitative assessment of segmental volume and radii of intrathoracic airway trees imaged by multi-row detector spiral CT. Am J Respir Crit Care Med 2003; 167:A846.
44. Hoffman E, Saba O, McLennan G, et al. Regional 3-D airway geometry in normal humans by use of multi-row detector computed tomography. Am J Respir Crit Care Med 2003; 167:A846.
45. Coxson HO, Patel BD, Nakano Y, et al. The role of emphysema and airway wall dimensions in chronic obstructive pulmonary disease (COPD). Am J Respir Crit Care Med 2003; 167:A81.
46. Uppaluri R, Mitsa T, Sonka M, Hoffman EA, McLennan G. Quantification of pulmonary emphysema from lung CT images using texture analysis. Am J Respir Crit Care Med 1997; 156:248–254.
47. Uppaluri R, Hoffman EA, Sonka M, Hunninghake GW, McLennan G. Interstitial lung disease: a quantitative study using the adoptive multiple feature method. Am J Respir Crit Care Med 1999; 159:519–525.
48. Uppaluri R, Hoffman EA, Sonka M, Hartley P, Hunninghake GW, McLennan G. Computer recognition of regional lung disease patterns. Am J Respir Crit Care Med 1999; 160:648–654.
49. Mishima M, Hirai T, Itoh H, et al. Complexity of terminal airspace geometry assessed by lung computed tomography in normal subjects and patients with chronic obstructive pulmonary disease. Proc Natl Acad Sci U S A 1999; 96:8829–8834.
50. Bentley MD, Lerman LO, Hoffman EA, Fiksen-Olsen MJ, Ritman EL, Romero JC. Measurement of renal perfusion and blood flow with fast computed tomography. Circ Res 1994; 74:945–951.
51. Wolfkiel CJ, Ferguson JL, Chomka EV, et al. Measurement of myocardial blood flow by ultrafast computed tomography. Circ 1987; 76:1262–1273.
52. Zierler KL. Equations for measuring blood flow by external monitoring of radioisotopes. Circ Res 1965; 16:309–321.
53. Hoffman EA, Tajik JK, Kugelmass SD. Matching pulmonary structure and perfusion via combined dynamic multislice CT and thin-slice high-resolution CT. Comput Med Imaging Graph 1995; 19:101–112.
54. Chulho W, Chon D, Tajik J, et al. CT-based assessment of regional pulmonary microvascular blood flow parameters. J Appl Physiol 2003; 94:2483–2493.
55. Samrah S, McLennan G, Chon D, Beck K, Ross A, Hoffman E. Multi-row detector CT-based measures of microvascular mean transit times and parenchymal texture as an early marker of inflammatory processes leading to emphysema. Am J Respir Crit Care Med 2003; 167: A874.
56. Gur D, Drayer BP, Borovetz HS, Griffith BP, Hardesty RL, Wolfson SK. Dynamic computed tomography of the lung: regional ventilation measurements. J Comp Asst Tomog 1979; 3:749–753.
57. Gur D, Shabason L, Borovetz HS, et al. Regional pulmonary ventilation measurements by xenon enhanced dynamic computed tomography: an update. J Comp Asst Tomog 1981; 5:678–683.
58. Marcucci C, Nyhan D, Simon B. Distribution of pulmonary ventilation using Xe-enhanced computed tomography is prone and supine dogs. J Appl Physiol 2001; 90:421–430.
59. Simon B. Non-invasive imaging of regional lung function using x-ray computed tomography. J Clin Monit Comput 2000; 16:433–442.
60. Tajik JK, Tran BQ, Hoffman EA. Xenon enhanced CT imaging of local pulmonary ventilation. SPIE Med Imaging Physiol Function 1996; 2709:40–54.
61. Simon B, Marcucci C, Fung M, Lele SR. Parameter estimation and confidence intervals for Xe-CT ventilation studies: a Monte Carlo approach. J Appl Physiol 1998; 84:709–716.
62. Tajik JK, Chon D, Won C, Tran BQ, Hoffman EA. Subsecond multisection CT of regional pulmonary ventilation. Acad Radiol 2002; 9:130–146.